

## Self-Powered Solar-Blind Photodetectors Based on $\alpha/\beta$ Phase Junction of $\text{Ga}_2\text{O}_3$

D.Y. Guo<sup>1,2,\*</sup>, K. Chen,<sup>1</sup> S.L. Wang,<sup>1</sup> F.M. Wu,<sup>1,†</sup> A.P. Liu,<sup>1</sup> C.R. Li,<sup>1</sup> P.G. Li,<sup>3</sup> C.K. Tan,<sup>4</sup> and W.H. Tang<sup>3,‡</sup>

<sup>1</sup>Center for Optoelectronics Materials and Devices & Key Laboratory of Optical Field Manipulation of Zhejiang Province, Department of Physics, Zhejiang Sci-Tech University, Hangzhou 310018, China

<sup>2</sup>State Key Lab of Silicon Materials, Zhejiang University, Hangzhou 310027, China

<sup>3</sup>Information Functional Materials and Devices & State Key Laboratory of Information Photonics and Optical Communications, School of Science, Beijing University of Posts and Telecommunications, Beijing 100876, China

<sup>4</sup>Department of Electrical and Computer Engineering, Clarkson University, Potsdam, New York 13699, USA

(Received 28 August 2019; revised manuscript received 27 December 2019; accepted 4 February 2020; published 20 February 2020)

Self-powered  $\text{Ga}_2\text{O}_3$ -based solar-blind photodetectors have received attention recently due to the increased demand for energy saving, miniaturization, and high efficiency in devices. An ideal device structure consisting of a  $\text{Ga}_2\text{O}_3$ -based  $p$ - $n$  junction is still difficult to obtain, since  $p$ -type doping is a major challenge. Although self-powered devices based on heterojunction are promising, there are two fatal disadvantages: (1) photosensitivity of the non-solar-blind region, on account of the narrower band gap of the heterojunction materials; and (2) poor quality of the epitaxial film due to lattice mismatch. In view of the various polymorphs of  $\text{Ga}_2\text{O}_3$ , we propose constructing a structure consisting of a  $\text{Ga}_2\text{O}_3$  phase junction with  $\alpha$  and  $\beta$  phases ( $\alpha/\beta$  phase junction) for self-powered solar-blind photodetectors. The small lattice mismatch and similar band gap between  $\alpha$ - and  $\beta$ - $\text{Ga}_2\text{O}_3$  will solve the two problems outlined above. The formation of  $\alpha$ - and  $\beta$ - $\text{Ga}_2\text{O}_3$  is expected to result in a type-II band alignment, promoting separation of photogenerated carriers, which transfer through the junction to the corresponding electrodes. Herein, the  $\alpha/\beta$  phase junction of  $\text{Ga}_2\text{O}_3$  vertically aligned nanorod arrays with a thickness-controllable  $\beta$ - $\text{Ga}_2\text{O}_3$  shell layer are fabricated by a low-cost and simple process of hydrothermal and postannealing treatment. Two different types of self-powered  $\alpha/\beta$ - $\text{Ga}_2\text{O}_3$  phase junction-based photodetectors, in the form of solid-state type and photoelectrochemical type, are constructed and realized. Our analysis shows that the constructed photodetectors are capable of highly efficient detection of solar-blind signal without any bias voltage. This work demonstrates the usefulness of using the  $\alpha/\beta$ - $\text{Ga}_2\text{O}_3$  phase junction in a self-powered solar-blind photodetector, which is not only energy efficient, but also potentially workable in outer space, at the south and north pole, and other harsh environments without external power for a long time.

DOI: 10.1103/PhysRevApplied.13.024051

### I. INTRODUCTION

Solar-blind photodetectors based on  $\text{Ga}_2\text{O}_3$  semiconductor, with high photosensitivity and low false-alarm rate, have attracted great interest recently due to their wide potential applications in military fields (such as ultraviolet communication, missile early warning and tracking, rocket tail-flame detection, and high-energy physics) and civilian fields (such as sterilization ultraviolet-intensity detection, biological medicine, fire warning, high-voltage corona detection, and ozone-hole monitoring) [1–5]. With the rapid development of technological society, devices are

gradually tailored to possessing characteristics of energy saving, miniaturization, and high efficiency, because traditional energy sources are unable to meet the increasing consumption demand of human beings [6]. To satisfy these demands,  $\text{Ga}_2\text{O}_3$  self-powered photodetectors based on the junction effect (such as heterojunctions, Schottky junctions, and  $p$ - $n$  junctions), which can separate electron-hole pairs with a built-in electric field, have developed rapidly [7–13]. Schottky-type devices are unsatisfactory due to low light transmission with the traditional common metal used as the upper electrode and the complex preparation process of the Schottky contact because of the large surface states of  $\beta$ - $\text{Ga}_2\text{O}_3$  [7,8]. Although devices based on  $p$ - $n$  junctions and heterojunctions exhibit appropriate photoelectric performance, there are two fatal disadvantages [9–13]: (1) the photodetection area is widened to the

\*dyguo@zstu.edu.cn

†fmw@zstu.edu.cn

‡whtang@bupt.edu.cn

non-solar-blind ultraviolet region because the band gap of the heterojunction material used is narrower than that of  $\beta$ - $\text{Ga}_2\text{O}_3$ ; and (2) high-quality epitaxial film is difficult to obtain due to the lattice mismatch between materials. For example, a self-powered photodetector based on the  $\text{GaN}/\text{Sn}:\text{Ga}_2\text{O}_3$  *p-n* junction, with a superhigh photoresponsivity of 3.05 A/W to illumination at 254 nm, has been fabricated in our previous work, but it also shows photosensitivity to the ultraviolet region, with a maximum wavelength of 370 nm [9]. Theoretically, the most ideal device structure is the homojunction structure of *p*-type and *n*-type  $\text{Ga}_2\text{O}_3$ . Intrinsic  $\beta$ - $\text{Ga}_2\text{O}_3$  shows *n*-type conductivity, the carrier concentration of which can be tuned from  $10^{17}$  to  $10^{20} \text{ cm}^{-3}$  through doping [14]. Grillo *et al.* achieved high field-emission current density from  $\beta$ - $\text{Ga}_2\text{O}_3$  nanopillars [15]. However, *p*-type  $\text{Ga}_2\text{O}_3$  is difficult to obtain due to the self-compensating effect [16].

In view of  $\text{Ga}_2\text{O}_3$  having various crystal structures (such as  $\alpha$ ,  $\beta$ ,  $\gamma$ ,  $\delta$ , and  $\epsilon$ ) and easy phase transformation [1,14,17–19], we propose constructing a  $\text{Ga}_2\text{O}_3$  phase junction structure with  $\alpha$  and  $\beta$  phases ( $\alpha/\beta$  phase junction) for self-powered solar-blind photodetectors. The advantages of small lattice mismatch [for example, the (110) plane of  $\alpha$ - $\text{Ga}_2\text{O}_3$  and the (310) plane of  $\beta$ - $\text{Ga}_2\text{O}_3$  with a lattice mismatch of only 3%] [19], and similar band gap between  $\alpha$ - and  $\beta$ - $\text{Ga}_2\text{O}_3$ , will solve the two abovementioned problems persisting in  $\text{Ga}_2\text{O}_3$ -based heterojunction devices. In addition, the type-II band alignment formed through the  $\alpha/\beta$  phase junction will promote effective separation of photogenerated carriers, which then transfer to the corresponding electrodes [20]. A self-powered photodetector based on the  $\text{Ga}_2\text{O}_3$   $\alpha/\beta$  phase junction is expected to realize the detection of a solar-blind light signal with zero-power consumption, which is not only energy efficient, but also potentially workable in different environments, including outer space, at the south or north pole, and other harsh environment without external power for a long time.

Herein, core-shell thickness-controllable  $\alpha/\beta$  phase junctions of  $\text{Ga}_2\text{O}_3$  vertically aligned nanorod arrays (NRAs) are fabricated by a low-cost, simple, and repeatable process of hydrothermal and postannealing treatment. Two different types, photoelectrochemical and solid state, of self-powered solar-blind photodetectors based on  $\alpha/\beta$ - $\text{Ga}_2\text{O}_3$  phase junction NRAs are constructed and investigated.

## II. EXPERIMENT

A schematic illustration of the fabrication process of  $\alpha/\beta$ - $\text{Ga}_2\text{O}_3$  phase junction NRAs is shown in Fig. 1. The ordered GaOOH NRAs are grown on fluorine-doped tin oxide (FTO) substrates by a hydrothermal method. Details of the preparation process were described in our previous work [21,22], with the exception that the seed layer

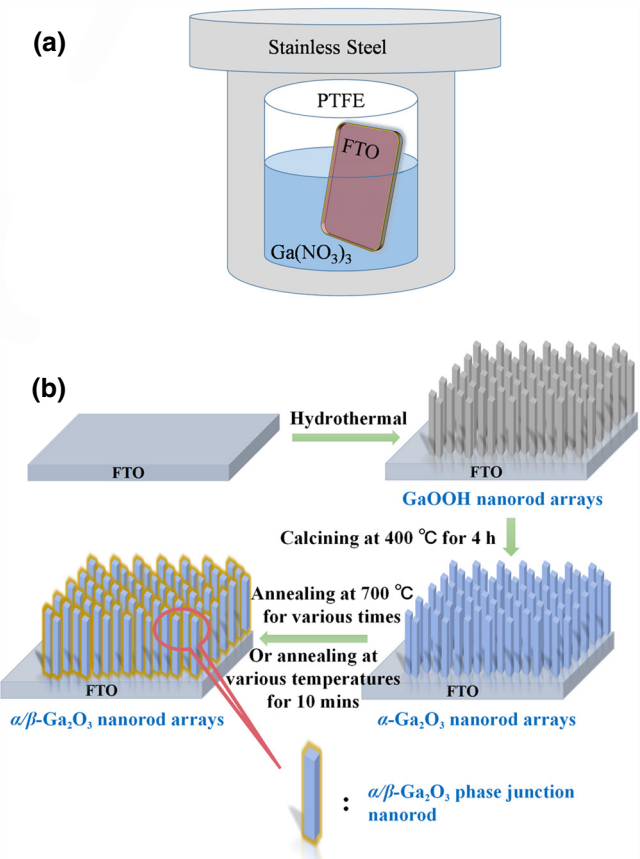
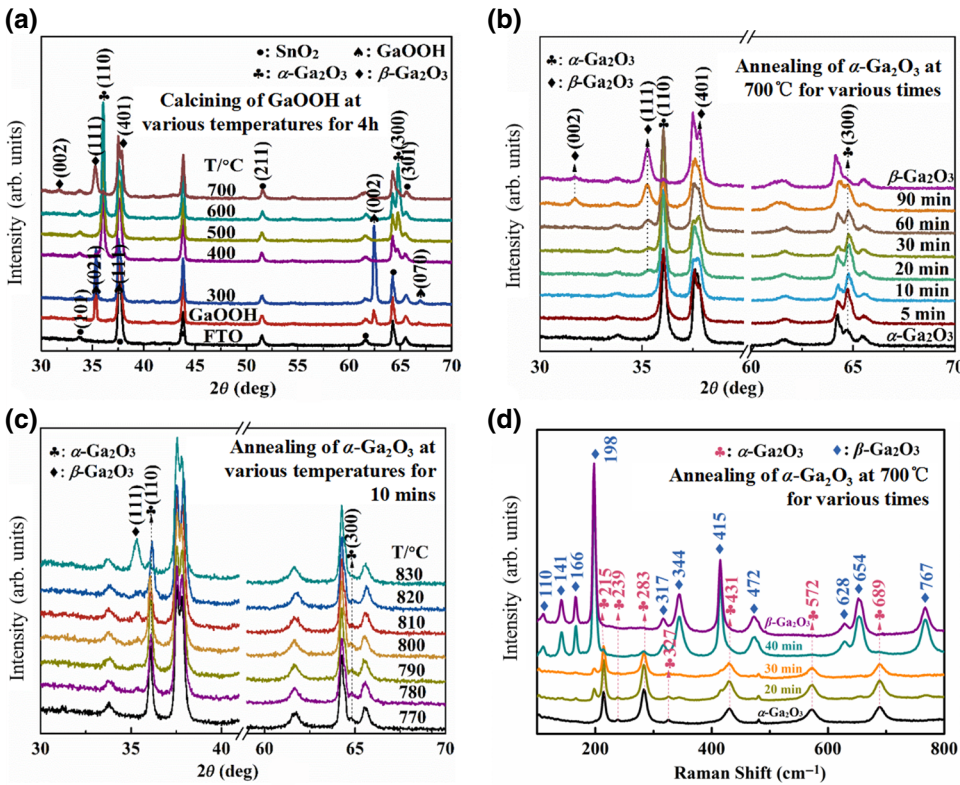


FIG. 1. Schematic diagrams of hydrothermal method (a) and preparation process (b) of  $\alpha/\beta$ - $\text{Ga}_2\text{O}_3$  phase junction NRAs.

was not used in this work. The effects of the growth solution concentration and growth time on the morphology of GaOOH NRAs are shown in Figs. S1 and S2 within the Supplemental Material [23]. FTO substrates recline inside a container of polytetrafluoroethylene (PTFE) under the optimum growth condition of a 0.3 g/30 ml  $\text{Ga}(\text{NO}_3)_3$  solution and heated at 150 °C for 12 h in an oven, as shown in Fig. 1(a). To explore the phase transition temperature of  $\text{Ga}_2\text{O}_3$ , the GaOOH NRAs are annealed in air for 4 h at various temperatures, ranging from 300 to 700 °C with an interval of 100 °C.

## III. RESULTS AND DISCUSSION

From the XRD patterns of Fig. 2(a),  $\alpha$ - and  $\beta$ - $\text{Ga}_2\text{O}_3$  can be obtained by annealing at 400 and 700 °C, respectively [24,25]. The thermogravimetric curves of GaOOH NRAs show consistent results (see Fig. S3 within the Supplemental Material [23]). Herein,  $\alpha/\beta$  phase junction  $\text{Ga}_2\text{O}_3$  NRAs with various thicknesses of  $\beta$ - $\text{Ga}_2\text{O}_3$  shell layers are fabricated by calcining GaOOH NRAs at 400 °C for 4 h followed by postannealing treatment at 700 °C for various times or postannealing at various temperatures for 10 min. As shown in Fig. 2(a), the peak located



at approximately 35.3°, corresponding to the (111) plane of β-Ga<sub>2</sub>O<sub>3</sub> (JCPDS file No. 43-1012), can be observed through annealing of α-Ga<sub>2</sub>O<sub>3</sub> NRAs at 700 °C for 20 min or under postannealing at 780 °C for 10 min [25]. The Raman spectra are consistent with the results of XRD [21,26]. In fact, a superthin β-Ga<sub>2</sub>O<sub>3</sub> shell layer should form under annealing at 700 °C for less than 20 min.

Figures 3(a) and 3(b) show the top-view and cross-section field-emission scanning electron microscope (FESEM) images, respectively, of α/β-Ga<sub>2</sub>O<sub>3</sub> phase junction NRAs under postannealing at 700 °C for 20 min. The prismlike tip of the nanorod is attributed to the orthorhombic structure of GaOOH NRAs (JCPDS file No. 06-0180) [22], which is consistent with the XRD observation in Fig. 2(a). The side lengths of the rhombus nanorods range from 100 to 500 nm, and the average height of these is approximately 1.5 μm. A porous structure like a sponge forms inside the nanorods due to the dehydration process of GaOOH NRAs, as described by 2GaOOH → α-Ga<sub>2</sub>O<sub>3</sub> + H<sub>2</sub>O, as shown in the bright-field TEM image in Fig. 3(c). The spacing between two adjacent lattice fringes of the outer shell layer are calculated to be about 2.54 and 2.88 Å, corresponding to (110) and (002) planes of β-Ga<sub>2</sub>O<sub>3</sub>, respectively, while that of the inner core bulk region is estimated to about 2.22 Å, corresponding to the (006) plane of α-Ga<sub>2</sub>O<sub>3</sub> [Fig. 3(d)].

The band gaps of α-Ga<sub>2</sub>O<sub>3</sub> and β-Ga<sub>2</sub>O<sub>3</sub> are about 4.96 and 4.66 eV, respectively, as estimated from the curves of  $(\alpha h\nu)^2$  versus  $h\nu$ , on the basis of the UV-vis

FIG. 2. XRD patterns of GaOOH NRAs calcined at various temperatures (a), α-Ga<sub>2</sub>O<sub>3</sub> NRAs calcined at 700 °C for various times (b), and α-Ga<sub>2</sub>O<sub>3</sub> NRAs calcined at various temperatures for 10 min. (d) Raman spectra of α-Ga<sub>2</sub>O<sub>3</sub> NRAs calcined at 700 °C for various times.

absorbance spectra (see Fig. S4 within the Supplemental Material [23]) [27]. Both of them present a strong absorption to deep-ultraviolet light, but not visible light, indicating their potential as suitable materials for solar-blind photodetection. The flat-band potentials of α-Ga<sub>2</sub>O<sub>3</sub> and β-Ga<sub>2</sub>O<sub>3</sub> are calculated to be -1.31 and -0.96 V (vs a saturated calomel electrode), respectively, according to the extrapolation of Mott-Schottky plots (see Fig. S5 within the Supplemental Material [23]) [27].

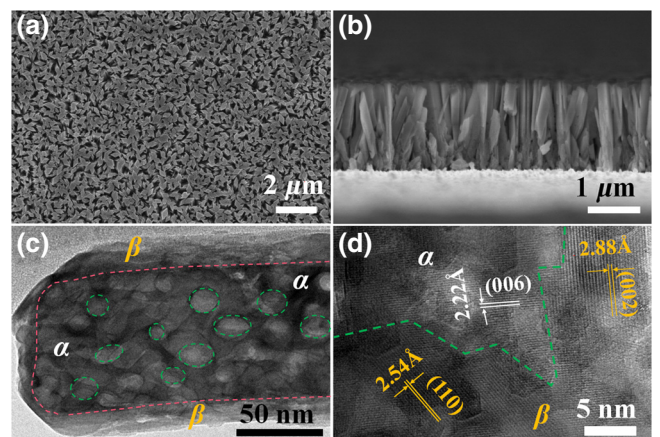


FIG. 3. Top view (a) and cross-section view (b) of FESEM images of α/β-Ga<sub>2</sub>O<sub>3</sub> phase junction NRAs. Bright-field TEM image (c) and HRTEM image (d) of α/β-Ga<sub>2</sub>O<sub>3</sub> phase junction NRAs.

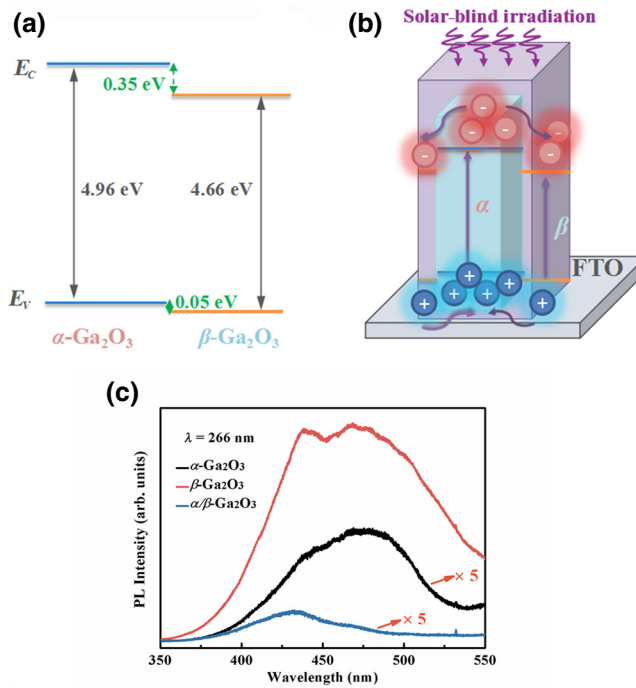


FIG. 4. (a) Energy band structure of  $\alpha/\beta\text{-Ga}_2\text{O}_3$  phase junction NRAs. (b) Transport of photogenerated carriers under solar-blind illumination. (c) PL spectra of  $\alpha\text{-Ga}_2\text{O}_3$ ,  $\beta\text{-Ga}_2\text{O}_3$ , and  $\alpha/\beta\text{-Ga}_2\text{O}_3$  phase junction nanorods excited by 266-nm laser.

Using the above results, the energy band alignment of  $\alpha/\beta\text{-Ga}_2\text{O}_3$  phase junction NRAs is illustrated in Fig. 4(a). Both the conduction-band potential ( $E_c$ ) and the valence-band potential ( $E_v$ ) of  $\alpha\text{-Ga}_2\text{O}_3$  are more positive than those of  $\beta\text{-Ga}_2\text{O}_3$ , exhibiting a type-II band alignment. As an estimation, the conduction-band offset ( $\Delta E_c$ ) is 0.35 eV, and the valence-band offset ( $\Delta E_v$ ) is 0.05 eV. We note that the conduction-band offset for the  $\alpha/\beta\text{-Ga}_2\text{O}_3$  phase junction is small. Considering factors such as defects and strains, which could induce changes to band alignment, further studies will be required to confirm the band offset values for the  $\alpha/\beta\text{-Ga}_2\text{O}_3$  phase junction.

The room-temperature photoluminescence (PL) spectra excited by a 266-nm laser are measured to check the effective separation of photogenerated carriers in the  $\alpha/\beta\text{-Ga}_2\text{O}_3$  phase junction. The PL spectra of  $\alpha\text{-Ga}_2\text{O}_3$ ,  $\beta\text{-Ga}_2\text{O}_3$ , and  $\alpha/\beta\text{-Ga}_2\text{O}_3$  phase junction nanorod powders are shown in the Fig. 4(c) for comparison, which are scraped from the vertically aligned nanorod arrays grown on the FTO substrates. The same weight of these nanorod powders are used here. All of them show a broad visible emission band from 350 to 550 nm, which is usually attributed to the recombination of carriers through defect states, such as oxygen vacancies [28,29]. Notably, the PL intensity for the  $\alpha/\beta\text{-Ga}_2\text{O}_3$  phase junction is significantly inhibited. This phenomenon could potentially be attributed to the type-II band alignment of the  $\alpha/\beta\text{-Ga}_2\text{O}_3$  phase

junction, which indicates that the photogenerated electron-hole pairs are separated into  $\beta\text{-Ga}_2\text{O}_3$  and  $\alpha\text{-Ga}_2\text{O}_3$  (electrons in  $\beta\text{-Ga}_2\text{O}_3$ , while holes are in  $\alpha\text{-Ga}_2\text{O}_3$ ). When solar-blind light illuminates the  $\alpha/\beta\text{-Ga}_2\text{O}_3$  phase junction NRAs, the high-energy deep-ultraviolet light will excite electrons into the conduction band, leaving holes in the valence band of both  $\alpha\text{-Ga}_2\text{O}_3$  and  $\beta\text{-Ga}_2\text{O}_3$ . Based on the type-II band alignment, the photogenerated electrons in the conduction band of  $\alpha\text{-Ga}_2\text{O}_3$  will transfer to the conduction band of  $\beta\text{-Ga}_2\text{O}_3$ , while the photogenerated holes will transfer from the  $\beta$  phase to the  $\alpha$  phase, as driven by the potential difference caused by the band level differences between them, as shown in Fig. 4(b).

Based on the efficient spontaneous separation of the photogenerated electron-hole pairs in the  $\alpha/\beta\text{-Ga}_2\text{O}_3$  phase junction, and some advantages of massive surface-to-volume ratio, low optical reflectivity, and efficient coupling with incident light of NRAs [8,29,30], the  $\alpha/\beta\text{-Ga}_2\text{O}_3$  phase junction NRAs are appropriate materials for self-powered solar-blind photodetectors. As shown in Fig. 5, solid-state-type and photoelectrochemical-type devices are designed for  $\alpha/\beta\text{-Ga}_2\text{O}_3$  phase junction self-powered solar-blind photodetectors. For the solid-state-type device, the rectifying characteristics are observed in the  $I-V$  curves, with a simple device structure of Ti/Au as the top electrode (see Fig. S6 within the Supplemental Material [23]). The photocurrent to 254 nm ultraviolet light increases concomitantly with the increase of the light intensity (see Fig. S6 within the Supplemental Material [23]). One possible direction in the future is to use a graphene monolayer or Ag-nanowire film as the top electrode due to their high transmittance of deep-ultraviolet light [31–33]. However, there is a drawback for the solid-state-type device: the photogenerated carriers cannot be efficiently separated and transferred, since the top electrodes of the graphene monolayer or Ag-nanowire film is in contact only with part of the upper end of the nanorods, which is attributed to the unevenness of the NRAs. In addition, graphene or Ag will be contactless with the perimeter of the nanorods [30]. To solve this issue, a photoelectrochemical-type device is assembled using the  $\alpha/\beta\text{-Ga}_2\text{O}_3$  phase junction NRAs as the active photoanode, a highly conductive material, such as platinum foil, as the counter electrode, and 0.5 M aqueous solution of  $\text{Na}_2\text{SO}_4$  as the electrolyte. This design exhibits great potential, on account of its large contact area of the solid-liquid interface and simple manufacturing process, as shown in Fig. 5(b) [21,30,34]. The suitably distributed gaps between the NRAs are conducive to penetration of the electrolyte [Fig. 3(a)]. Also, the porous structure of nanorods [Fig. 3(c)] can provide large active sites at the solid-liquid interface for the separation of electron-hole pairs. The current densities in the linear sweep voltammetry curves show rectification characteristics, which can be attributed to the energy band bending of the  $\alpha/\beta\text{-Ga}_2\text{O}_3$  phase junction, as well as the interface

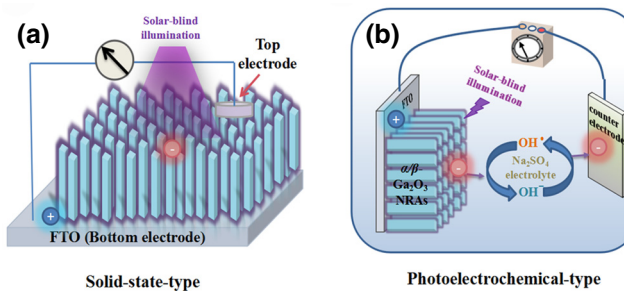


FIG. 5. Photoelectrochemical-type (a) and solid-state-type (b) self-powered solar-blind photodetectors based on  $\alpha/\beta$ -Ga<sub>2</sub>O<sub>3</sub> phase junction NRAs.

of the Ga<sub>2</sub>O<sub>3</sub>-electrolyte solid-liquid heterojunctions, as shown in Fig. S7 within the Supplemental Material [23]. Although  $\alpha$ -Ga<sub>2</sub>O<sub>3</sub> NRA photoelectrochemical-type photodetectors also exhibit self-powered behavior,  $\alpha/\beta$ -Ga<sub>2</sub>O<sub>3</sub> phase junction devices show superior photoelectric performance at a bias of 0 V (see Fig. S7 within the Supplemental Material [23]). The photoelectric performance of the  $\alpha/\beta$ -Ga<sub>2</sub>O<sub>3</sub> phase junction NRA photoelectrochemical-type photodetectors increases first and then decreases with increasing  $\beta$ -Ga<sub>2</sub>O<sub>3</sub> shell-layer thickness, which reaches a maximum value by annealing of  $\alpha$ -Ga<sub>2</sub>O<sub>3</sub> NRAs at 700 °C for 10 min (see Fig. S7 within the Supplemental Material [23]). These results show that the  $\alpha/\beta$ -Ga<sub>2</sub>O<sub>3</sub> phase junction NRA based solar-blind photodetectors can work without an external power source and therefore, make them self-powered devices, which have potentially important applications, such as secure ultraviolet communication and space detection.

#### IV. CONCLUSIONS

The size, length, and shell-layer-thickness controllable  $\alpha/\beta$  phase junction of Ga<sub>2</sub>O<sub>3</sub> vertically aligned NRAs are grown on FTO substrates through a simple and low-cost method of hydrothermal and postannealing treatments. The thickness of the  $\beta$ -Ga<sub>2</sub>O<sub>3</sub> shell layer increases with increasing annealing time or temperature. The significant inhibition of the PL intensity in the  $\alpha/\beta$  Ga<sub>2</sub>O<sub>3</sub> phase junction compared with that of the pure phase indicates that the photogenerated electron-hole pairs can be effectively separated. Two different types of photodetector are demonstrated: photoelectrochemical and solid state. Both the photoelectrochemical-type and solid-state-type photodetectors based on  $\alpha/\beta$ -Ga<sub>2</sub>O<sub>3</sub> phase junction NRAs exhibit self-powered and solar-blind photoelectric characteristics. Our work demonstrates a promising device structure for developing a self-powered solar-blind photodetector.

#### ACKNOWLEDGMENTS

This work is supported by the National Natural Science Foundation of China (Grants No. 61704153 and

No. 61774019), the Zhejiang Public Service Technology Research Program/Analytical Test (Grant No. LGC19F040001), the Natural Science Foundation of Zhejiang Province (Grant No. LY20F040005), the Visiting Scholar Foundation of State Key Lab of Silicon Materials (Grant No. SKL2019-08), and the Fundamental Research Funds of Zhejiang Sci-Tech University (Grants No. 2019Q061 and No. 2019Q067).

D. Y. Guo and K. Chen contributed equally to this work.

- [1] D. Y. Guo, P. G. Li, Z. W. Chen, Z. P. Wu, and W. H. Tang, Ultra-wide bandgap semiconductor of  $\beta$ -Ga<sub>2</sub>O<sub>3</sub> and its research progress of deep ultraviolet transparent electrode and solar-blind photodetector, *Acta Phys. Sin.-Ch. Ed.* **68**, 078501 (2019).
- [2] X. H. Chen, F. F. Ren, S. L. Gu, and J. D. Ye, Review of gallium-oxide-based solar-blind ultraviolet photodetectors, *Photonics Res.* **7**, 381 (2019).
- [3] Y. Qin, S. B. Long, H. Dong, Q. M. He, G. Z. Jian, Y. Zhang, X. H. Hou, P. J. Tan, Z. F. Zhang, H. B. Lv, Q. Liu, and M. Liu, Review of deep ultraviolet photodetector based on gallium oxide, *Chin. Phys. B* **28**, 018501 (2019).
- [4] D. Y. Guo, Z. P. Wu, P. G. Li, Y. H. An, H. Liu, X. C. Guo, H. Yan, G. F. Wang, C. L. Sun, L. H. Li, and W. H. Tang, Fabrication of  $\beta$ -Ga<sub>2</sub>O<sub>3</sub> thin films and solar-blind photodetectors by laser MBE technology, *Opt. Mater. Express* **4**, 1067 (2014).
- [5] D. Y. Guo, Z. P. Wu, Y. H. An, X. C. Guo, X. L. Chu, C. L. Sun, L. H. Li, P. G. Li, and W. H. Tang, Oxygen vacancy tuned Ohmic-Schottky conversion for enhanced performance in  $\beta$ -Ga<sub>2</sub>O<sub>3</sub> solar-blind ultraviolet photodetectors, *Appl. Phys. Lett.* **105**, 023507 (2014).
- [6] W. W. Zhong, J. D. Huang, S. Q. Liang, J. Liu, Y. J. Li, G. M. Cai, Y. Jiang, and J. Liu, New prelithiated V<sub>2</sub>O<sub>5</sub> superstructure for lithium-ion batteries with long cycle life and high power, *ACS Energy Lett.* **5**, 31 (2020).
- [7] T. Oshima, T. Okuno, N. Arai, N. Suzuki, S. Ohira, and S. Fujita, Vertical solar-blind deep-ultraviolet schottky photodetectors based on  $\beta$ -Ga<sub>2</sub>O<sub>3</sub> substrates, *Appl. Phys. Express* **1**, 011202 (2008).
- [8] X. Chen, K. W. Liu, Z. Z. Zhang, C. R. Wang, B. H. Li, H. F. Zhao, D. X. Zhao, and D. Z. Shen, Self-powered solar-blind photodetector with fast response based on Au/ $\beta$ -Ga<sub>2</sub>O<sub>3</sub> nanowires array film Schottky junction, *ACS Appl. Mater. Inter.* **8**, 4185 (2016).
- [9] D. Y. Guo, Y. L. Su, H. Z. Shi, P. G. Li, N. Zhao, J. H. Ye, S. L. Wang, A. P. Liu, Z. W. Chen, C. R. Li, and W. H. Tang, Self-powered ultraviolet photodetector with super high photoresponsivity (3.05 A/W) based on the GaN/Sn : Ga<sub>2</sub>O<sub>3</sub> *pn* junction, *ACS Nano* **12**, 12827 (2018).
- [10] D. Y. Guo, H. Liu, P. G. Li, Z. P. Wu, S. L. Wang, C. Cui, C. R. Li, and W. H. Tang, Zero-power-consumption solar-blind photodetector based on  $\beta$ -Ga<sub>2</sub>O<sub>3</sub>/NSTO heterojunction, *ACS Appl. Mater. Inter.* **9**, 1619 (2017).
- [11] P. G. Li, H. Z. Shi, K. Chen, D. Y. Guo, W. Cui, Y. S. Zhi, S. L. Wang, Z. P. Wu, Z. W. Chen, and W. H. Tang, Construction of GaN/Ga<sub>2</sub>O<sub>3</sub> *pn* junction for an extremely

- high responsivity self-powered UV photodetector, *J. Mater. Chem. C* **5**, 10562 (2017).
- [12] S. Nakagomi, T. Momo, S. Takahashi, and Y. Kokubun, Deep ultraviolet photodiodes based on  $\beta$ -Ga<sub>2</sub>O<sub>3</sub>/SiC heterojunction, *Appl. Phys. Lett.* **103**, 072105 (2013).
- [13] S. Nakagomi, T. Sato, Y. Takahashi, and Y. Kokubun, Deep ultraviolet photodiodes based on the  $\beta$ -Ga<sub>2</sub>O<sub>3</sub>/GaN heterojunction, *Sensor. Actuat. A: Phys.* **232**, 208 (2015).
- [14] D. Y. Guo, Q. X. Guo, Z. W. Chen, Z. P. Wu, P. G. Li, and W. H. Tang, Review of Ga<sub>2</sub>O<sub>3</sub> based optoelectronic devices, *Mater. Today Phys.* **11**, 100157 (2019).
- [15] A. Grillo, J. Barrat, Z. Galazka, M. Passacantando, F. Giubileo, L. Iemmo, G. Luongo, F. Urban, C. Dubourdieu, and A. D. Bartolomeo, High field-emission current density from  $\beta$ -Ga<sub>2</sub>O<sub>3</sub> nanopillars, *Appl. Phys. Lett.* **114**, 193101 (2019).
- [16] Y. L. Su, D. Y. Guo, J. H. Ye, H. L. Zhao, Z. Wang, S. L. Wang, P. G. Li, and W. H. Tang, Deep level acceptors of Zn-Mg divalent ions dopants in  $\beta$ -Ga<sub>2</sub>O<sub>3</sub> for the difficulty to p-type conductivity, *J. Alloy. Compd.* **782**, 299 (2019).
- [17] D. Y. Guo, Y. P. Qian, Y. L. Su, H. Z. Shi, P. G. Li, J. T. Wu, S. L. Wang, C. Cui, and W. H. Tang, Evidence for the bias-driven migration of oxygen vacancies in amorphous non-stoichiometric gallium oxide, *AIP Adv.* **7**, 065312 (2017).
- [18] D. Y. Guo, X. Y. Qin, M. Lv, H. Z. Shi, Y. L. Su, G. S. Yao, S. L. Wang, C. R. Li, P. G. Li, and W. H. Tang, Decrease of oxygen vacancy by Zn-doped for improving solar-blind photoelectric performance in  $\beta$ -Ga<sub>2</sub>O<sub>3</sub> thin films, *Electron. Mater. Lett.* **13**, 483 (2017).
- [19] X. Wang, Q. Xu, M. R. Li, S. Shen, X. L. Wang, Y. C. Wang, Z. C. Feng, J. Y. Shi, H. X. Han, and C. Li, Photocatalytic overall water splitting promoted by an  $\alpha$ - $\beta$  phase junction on Ga<sub>2</sub>O<sub>3</sub>, *Angew. Chem. Int. Ed.* **51**, 13089 (2012).
- [20] Y. Wang, Q. Wang, X. Zhan, F. Wang, M. Safdar, and J. He, Visible light driven type II heterostructures and their enhanced photocatalysis properties: A review, *Nanoscale* **5**, 8326 (2013).
- [21] C. R. He, D. Y. Guo, K. Chen, S. L. Wang, J. Q. Shen, N. Zhao, A. P. Liu, Y. Y. Zheng, P. G. Li, Z. P. Wu, C. R. Li, F. M. Wu, and W. H. Tang,  $\alpha$ -Ga<sub>2</sub>O<sub>3</sub> nanorod array-Cu<sub>2</sub>O microsphere pn junctions for self-powered spectrum-distinguishable photodetectors, *ACS Appl. Nano Mater.* **2**, 4095 (2019).
- [22] K. Chen, C. R. He, D. Y. Guo, S. L. Wang, Z. W. Chen, J. Q. Shen, P. G. Li, and W. H. Tang, Low-voltage-worked photodetector based on Cu<sub>2</sub>O/GaOOH shell-core heterojunction nanorod arrays, *J. Alloy. Compd.* **755**, 199 (2018).
- [23] See the Supplementary Material at <http://link.aps.org/supplemental/10.1103/PhysRevApplied.13.024051> for the details of materials' characterization and device measurements, the FESEM images of GaOOH NRAs under various growth conditions, the thermogravimetric curve, the UV-vis absorption spectra, the Mott-Schottky plots, and the solar-blind photoelectric performance of the photoelectrochemical-type and solid-state-type self-powered photodetectors based on  $\alpha$ / $\beta$ -Ga<sub>2</sub>O<sub>3</sub> phase junction NRAs.
- [24] D. Y. Guo, X. L. Zhao, Y. S. Zhi, W. Cui, Y. Q. Huang, Y. H. An, P. G. Li, Z. P. Wu, and W. H. Tang, Epitaxial growth and solar-blind photoelectric properties of corundum-structured  $\alpha$ -Ga<sub>2</sub>O<sub>3</sub> thin films, *Mater. Lett.* **164**, 364 (2016).
- [25] D. Y. Guo, Z. P. Wu, P. G. Li, Q. J. Wang, M. Lei, L. H. Li, and W. H. Tang, Magnetic anisotropy and deep ultraviolet photoresponse characteristics in Ga<sub>2</sub>O<sub>3</sub> : Cr vermicular nanowire thin film nanostructure, *RSC Adv.* **5**, 12894 (2015).
- [26] R. Rao, A. M. Rao, B. Xu, J. Dong, S. Sharma, and M. K. Sunkara, Blueshifted Raman scattering and its correlation with the [110] growth direction in gallium oxide nanowires, *J. Appl. Phys.* **98**, 094312 (2005).
- [27] K. Chen, S. L. Wang, C. R. He, H. W. Zhu, H. L. Zhao, D. Y. Guo, Z. W. Chen, J. Q. Shen, P. G. Li, A. P. Liu, C. R. Li, F. M. Wu, and W. H. Tang, Photoelectrochemical self-powered solar-blind photodetectors based on Ga<sub>2</sub>O<sub>3</sub> nanorod array/electrolyte solid/liquid heterojunctions with a large separation interface of photogenerated carriers, *ACS Appl. Nano Mater.* **2**, 6169 (2019).
- [28] F. B. Zhang, H. O. Li, Y. T. Cui, G. L. Li, and Q. X. Guo, Evolution of optical properties and band structure from amorphous to crystalline Ga<sub>2</sub>O<sub>3</sub> films, *AIP Adv.* **8**, 045112 (2018).
- [29] D. Y. Guo, J. B. Wang, C. Cui, P. G. Li, X. L. Zhong, F. Wang, S. G. Yuan, K. D. Zhang, and Y. C. Zhou, Zno@TiO<sub>2</sub> core-shell nanorod arrays with enhanced photoelectrochemical performance, *Sol. Energy* **95**, 237 (2013).
- [30] T. He, X. D. Zhang, X. Y. Ding, C. Sun, Y. K. Zhao, Q. Yu, J. Q. Ning, R. X. Wang, G. H. Yu, S. L. Lu, K. Zhang, X. P. Zhang, and B. S. Zhang, Broadband ultraviolet photodetector based on vertical Ga<sub>2</sub>O<sub>3</sub>/GaN nanowire array with high responsivity, *Adv. Opt. Mater.* **7**, 1801563 (2019).
- [31] W. Zheng, R. Lin, J. Ran, Z. Zhang, X. Ji, and F. Huang, Vacuum-ultraviolet photovoltaic detector, *ACS Nano* **12**, 425 (2018).
- [32] S. Lin, H. Y. Wang, X. N. Zhang, D. Wang, D. Zu, J. N. Song, Z. L. Liu, Y. Huang, K. Huang, N. Tao, Z. W. Li, X. P. Bai, B. Li, M. Lei, Z. F. Yu, and H. Wu, Direct spray-coating of highly robust and transparent Ag nanowires for energy saving windows, *Nano Energy* **62**, 111 (2019).
- [33] S. Lin, H. Y. Wang, F. Wu, Q. M. Wang, X. P. Bai, D. Zu, J. N. Song, D. Wang, Z. L. Liu, Z. W. Li, N. Tao, K. Huang, M. Lei, B. Li, and H. Wu, Room-temperature production of silver-nanofiber film for large-area, transparent and flexible surface electromagnetic interference shielding, *npj Flex. Electron.* **3**, 6 (2019).
- [34] J. H. Zhang, S. J. Jiao, D. B. Wang, S. M. Ni, S. Y. Gao, and J. Z. Wang, Solar-blind ultraviolet photodetection of an  $\alpha$ -Ga<sub>2</sub>O<sub>3</sub> nanorod array based on photoelectrochemical self-powered detectors with a simple, newly-designed structure, *J. Mater. Chem. C* **7**, 6867 (2019).